ChemSusChem

Research Article
doi.org/10.1002/cssc.202202277

Chemistry Europe
European Chemical Societies Publishing

www.chemsuschem.org

VIP *Very Important Paper*

Concentration-Dependent Inhibition of Mesophilic PETases on Poly(ethylene terephthalate) Can Be Eliminated by Enzyme Engineering

Luisana Avilan,[a, b] Bruce R. Lichtenstein,[a, b] Gerhard König,[a, b] Michael Zahn,[a, b] Mark D. Allen,[a, b] Liliana Oliveira,[a, b] Matilda Clark,[a, b] Victoria Bemmer,[a, b] Rosie Graham,[a, b] Harry P. Austin,[c] Graham Dominick,[d] Christopher W. Johnson,[d] Gregg T. Beckham,[b, d] John E. McGeehan,[a, b] and Andrew R. Pickford*[a, b]

Enzyme-based depolymerization is a viable approach for recycling of poly(ethylene terephthalate) (PET). PETase from *Ideonella sakaiensis* (*Is*PETase) is capable of PET hydrolysis under mild conditions but suffers from concentration-dependent inhibition. In this study, this inhibition is found to be dependent on incubation time, the solution conditions, and PET surface area. Furthermore, this inhibition is evident in other mesophilic PET-degrading enzymes to varying degrees, independent of the level of PET depolymerization activity. The inhibition has no clear structural basis, but moderately thermostable *Is*PETase variants exhibit reduced inhibition, and the property is completely absent in the highly thermostable HotPETase, previously engineered by directed evolution, which simulations suggest results from reduced flexibility around the active site. This work highlights a limitation in applying natural mesophilic hydrolases for PET hydrolysis and reveals an unexpected positive outcome of engineering these enzymes for enhanced thermostability.

Introduction

The use of enzymes for polyester depolymerization has been proposed as a new chemical recycling strategy for this ubiquitous waste polymer. Some enzymes from the α/β-hydrolase superfamily, including promiscuous cutinases, are able to hydrolyze ester bonds in their natural substrates and are capable of depolymerizing synthetic polyesters including poly(ethylene terephthalate) (PET).[1] *Is*PETase from the mesophilic bacterium *Ideonella sakaiensis* hydrolyses PET into terephthalic acid (TPA), mono-2-hydroxyethyl terephthalate (MHET), ethylene glycol (EG), and small amounts of bis(2-hydroxyethyl) terephthalate (BHET).[2] *Is*PETase has been extensively studied and subject to protein engineering and directed evolution to improve its activity towards PET depolymerization and its thermostability.[3] Based on phylogenetic analysis and conserved structural features, bacterial *Is*PETase homologues have been classified as type I and II.[4] Type II enzymes have, among other features, an additional disulfide bond and an extended loop near the active site.[4] *Is*PETase and other enzymes previously characterized as mesophilic[5,6] belong to type II, while the thermophilic enzymes such as leaf compost cutinase (LCC) and the *Thermobifida fusca* cutinases belong to type I.[4] In addition, the type II enzyme class has been further divided into type IIa and IIb on the basis of differences within the extended loop and the active site cleft.[4]

The enzymes that break down PET are interfacial biocatalysts that act at the available scissile bonds on the plastic surface. The availability of these bonds for enzymatic hydrolysis is variable and dependent on, for example, their proximity to the polymer surface and the degree of polymer crystallinity.[7,8] Furthermore, bonds that are initially inaccessible to enzyme may be revealed as the polymer surface is eroded through enzymatic hydrolysis of solvent-exposed chains. Consequently, rather than employing the classical Michaelis-Menten formalism for soluble substrates, interfacial enzymatic efficiency against PET[7,8] is typically quantified using either a Langmuir adsorption-based analysis,[9–14] or an inverse Michaelis-Menten" approach;[12,15–17] the latter approach was first employed in the

[a] *Dr. L. Avilan, Dr. B. R. Lichtenstein, Dr. G. König, Dr. M. Zahn, Dr. M. D. Allen, L. Oliveira, M. Clark, Dr. V. Bemmer, R. Graham, Prof. J. E. McGeehan, Prof. A. R. Pickford*
Centre for Enzyme Innovation,
School of Biological Sciences,
Institute of Biological and Biomedical Sciences
University of Portsmouth,
Portsmouth PO1 2DY
(United Kingdom)
E-mail: andy.pickford@port.ac.uk

[b] *Dr. L. Avilan, Dr. B. R. Lichtenstein, Dr. G. König, Dr. M. Zahn, Dr. M. D. Allen, L. Oliveira, M. Clark, Dr. V. Bemmer, R. Graham, Dr. G. T. Beckham, Prof. J. E. McGeehan, Prof. A. R. Pickford*
BOTTLE Consortium
Golden, CO 80401 (United States)

[c] *Dr. H. P. Austin*
Institute of Biochemistry,
Department of Biotechnology & Enzyme Catalysis
University of Greifswald,
D-17487 Greifswald (Germany)

[d] *G. Dominick, Dr. C. W. Johnson, Dr. G. T. Beckham*
Renewable Resources and Enabling Sciences Center
National Renewable Energy Laboratory
Golden, CO 80401
(United States)

Supporting information for this article is available on the WWW under https://doi.org/10.1002/cssc.202202277

study of cellulose hydrolysis.[18,19] These two models are mathematically equivalent,[8,12] both relying on the experimental system exhibiting a hyperbolic relationship between the enzyme concentration and the reaction velocity, the latter being determined by the proportion of productively bound enzyme molecules at attackable sites on the polymer surface. However, the hyperbolic relationship between velocity and enzyme concentration is not present with *Is*PETase under certain experimental conditions.[2,15,20] Instead, the activity increases as a function of the enzyme concentration, until it reaches a maximum after which the activity decreases again; this may limit the industrial usefulness of an enzyme that would otherwise have appreciable activity at moderate temperatures. This inhibition of activity at high enzyme concentration has been also observed for TfCut2 digestion of PET film-derived nanoparticles,[11] and for other polymers such as poly(3-hydroxybutyrate) by enzymes from different sources[21,22] including *Fusarium solani* cutinase on immobilized substrates,[23] suggesting that it is an intrinsic property of some interfacial enzymatic reactions.

In this study, we focused on the enzyme concentration-dependent inhibition of *Is*PETase and eight homologous mesophilic enzymes from the type IIa and IIb subclasses to understand their performance in interfacial biocatalysis. We found that inhibition at high enzyme concentration is common in the mesophilic cutinases tested, that it is linked to protein flexibility, and that elevating the thermostability of mesophilic enzymes through engineering can mitigate this behavior. This knowledge may guide future attempts at modulating concentration-dependent inhibition of interfacial enzymes through protein engineering to maintain optimal rates of surface activities like plastic depolymerization.

Results

Inhibition of PET hydrolysis at high IsPETase concentration

We measured the PET hydrolase activity of *Is*PETase at 50–500 nM enzyme concentration and at pH 8.0 and 9.0 (Figure 1A,B); considering the 54.9 mm^2 surface area of the stadium shaped PET coupon and the molecular weight of *Is*PETase, this is equivalent to range of enzyme loading per PET surface area of 1.38–13.8 $\mu g\,cm^{-2}$. In agreement with previous reports,[15,20] the activity, reported as the sum of the aromatic products (BHET, MHET and TPA), increases to a maximum at between 50 and 100 nM *Is*PETase, and then falls at higher enzyme concentration. The inhibition percentage – defined as the ratio between the maximum product yield at any enzyme concentration and the product yield at 500 nM enzyme concentration (the maximum used) – is 72.9 ± 2.6% at pH 8.0, and 93 ± 0.9% at pH 9.0. Notably, the maximal activity (at 100 nM *Is*PETase concentration) is approximately 3-fold higher at pH 9.0 compared to pH 8.0 (Figure 1A,B). In the presence of dimethyl sulfoxide (DMSO), the concentration-dependent inhibition of *Is*PETase is diminished at pH 9.0 and eliminated at pH 8.0 (Figure 1C,D and Figure S1 in the Supporting Information). In addition, DMSO stimulates PET hydrolysis activity consistent

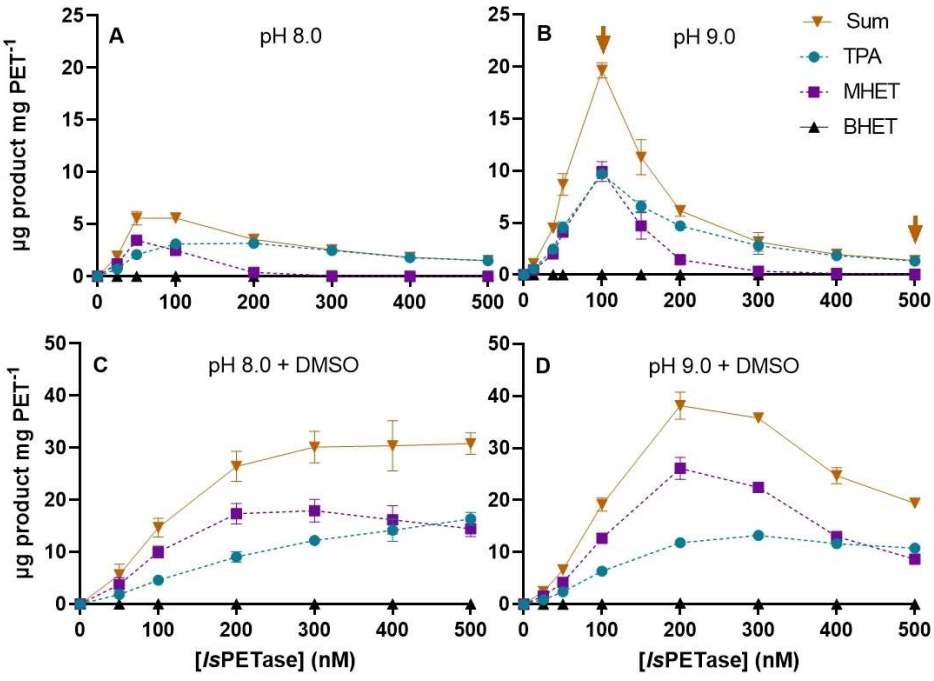

Figure 1. PET film hydrolysis as a function of *Is*PETase concentration. Amorphous PET films were incubated with different concentrations of *Is*PETase for 96 h at 30 °C in 50 mM KH_2PO_4/K_2HPO_4 at pH 8.0 (A,C) or 50 mM bicine at pH 9.0 (B,D). The reactions in (C) and (D) included 10% (v/v) DMSO. Values for TPA (blue), MHET (purple), BHET (black) and the sum of aromatic products (brown) are shown. Data are the means ± SD of triplicate reactions. The arrows in panel B indicate the points at which the level of inhibition (the ratio between maximum product and product at 500 nM enzyme) was quantified. The data for these plots are in Dataset S1.

with previous reports.[16] Here, maximal activity is increased approximately 5-fold at pH 8.0 (Figure 1A,C), and 2-fold at pH 9.0 (Figure 1B,D).

To investigate the temporal nature of concentration-dependent inhibition, we performed time-courses of *Is*PETase-mediated PET hydrolysis under those conditions where the phenomenon is strongest for this enzyme, that is, at pH 9.0 in the absence of DMSO (Figure S2 and Figure 2A,B). Under these conditions, significant inhibition of PET turnover activity at high enzyme concentration starts to become evident after approximately 1 h of incubation (Figure S3); the degree of inhibition rises above 50% after 2 h and is sustained at a high level throughout the remainder of the 4-day time-course (Figure 2C). During this period, the greatest degree of PET hydrolysis is witnessed for 50–100 nM *Is*PETase, with an enzyme loading of 2.75–5.51 μg cm^{-2}. This enzyme concentration-dependent inhibition is even more pronounced in the fusion of *Is*MHETase, an enzyme that hydrolyses MHET in *I. sakaiensis*,[2] and *Is*PETase.[24] This enzyme fusion exhibits 99 ± 0.1% inhibition at pH 8.0 (Figure S4). This acute susceptibility of *Is*PETase to concentration-dependent inhibition is evident for the individual aromatic products TPA and MHET and is stronger at 30 °C than 40 °C (Figure S5). Consistent with an earlier report,[2] the inhibition of MHET production at high enzyme concentration appears to be more pronounced than for TPA. Although MHETase activity was initially reported to be absent in *Is*PETase,[2] it has been subsequently observed during extended incubations.[25] Here, we measured detectable MHETase activity with 100 nM *Is*PETase, albeit at a rate approximately 280-times lower than for BHET hydrolysis (Figure S6). Moreover, the MHETase activity increases with the *Is*PETase concentration, confirming that the hydrolysis is enzymatic rather than spontaneous (Figure S6). The marked decline in observed MHET production is thus a consequence of both the inhibition of PET hydrolysis at high enzyme concentration and this intrinsic MHETase activity in *Is*PETase.

Inhibition of PET hydrolysis at high IsPETase concentration is a surface phenomenon

The observed concentration-dependent inhibition could potentially arise from aggregation of the enzyme in solution. To investigate this possibility, we analyzed the behavior of *Is*PETase in solution by analytical size exclusion chromatography (Figure S7). Across all concentrations tested (5 to 50 μM), *Is*PETase eluted as a single, narrow peak without any change in elution volume (and, hence, apparent MW), suggesting a consistent monomeric state. Furthermore, the rate of BHET hydrolysis does not decline at elevated *Is*PETase concentrations, as would be expected if the enzyme were aggregating in solution (Figure S8), so we conclude that the concentration-dependent inhibition is a surface phenomenon produced when enzyme molecules interact with each other following substrate binding.

Enzyme concentration-dependent inhibition is dependent on substrate surface area

To gain further insight into inhibition at high enzyme concentrations in *Is*PETase, we analyzed the dependence of PET hydrolysis activity on substrate surface area by varying the amorphous PET film solids loading. Iteratively doubling the solids loading from 2.1 wt% to 16.8 wt% (and, hence, iteratively halving the enzyme loading per surface area) resulted in a reduction in the inhibition (Figure 3A) with a concomitant increase of the enzyme concentration at which inhibition occurs. This shift in inhibitory enzyme concentration is consistent with the relief of inhibitory enzyme–enzyme interactions at the PET surface as enzyme density falls due to a reduced enzyme loading per surface area. In contrast, increasing the enzyme concentration in proportion to the PET loading strengthens the inhibition (Figure 3B).

These results indicate that adding more *Is*PETase enzyme in a digestion process does not increase PET hydrolysis, even at industrially relevant PET loadings of 10–20 wt%.[26–28]

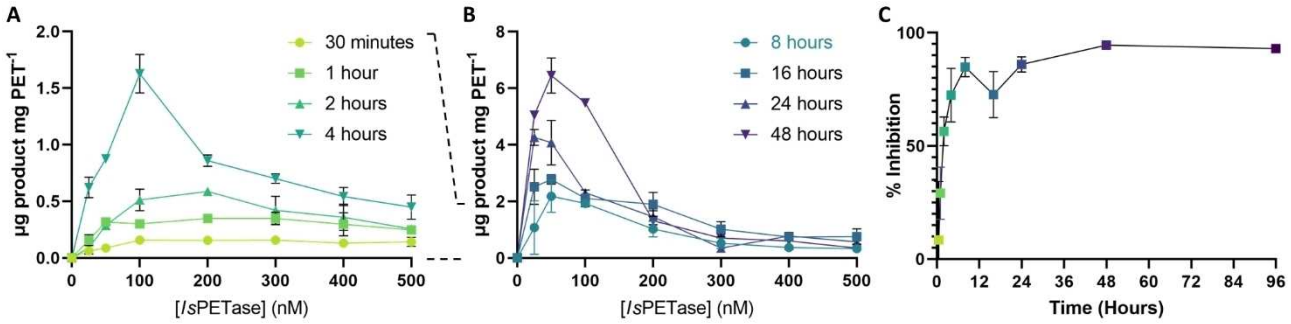

Figure 2. Enzyme concentration-dependent inhibition of *Is*PETase PET hydrolysis increases over time. Total aromatic product arising from PET film hydrolysis as a function of *Is*PETase concentration is shown for reaction incubation times of 30 min to 4 h (A) and 8 h to 48 h (B). Amorphous PET films were incubated with different concentrations of *Is*PETase for 30 °C in 50 mM bicine at pH 9.0. In each case, the sums of aromatic products are shown. Data are the means ± SD of triplicate reactions. Separate plots showing each individual aromatic product at each time point are provided in Figure S2. In (C), the level of inhibition (defined in Figure 1) is shown as a function of time. The data for these plots are given in Dataset S1.

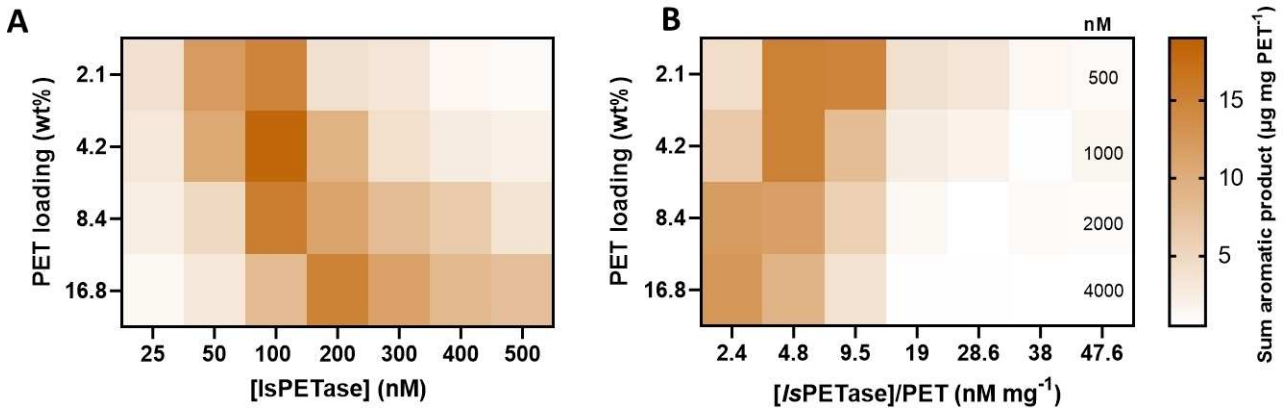

Figure 3. Heatmaps of *Is*PETase activity at various solids loadings of amorphous PET film. (A) Profile of the enzyme concentration dependence of the PET film hydrolysis at different PET film loading (wt%) with the same enzyme concentration range for each solids loading. (B) Profile of the enzyme concentration-dependent hydrolysis at different PET film loading (wt%) on the assay at constant ratio of enzyme concentration to substrate loading. In (B), the maximal enzyme concentration used for each PET loading is provided in the rightmost squares. Reactions were performed for 96 h at 30 °C in 50 mM bicine at pH 9.0. The sum of aromatic products is shown. The data for these plots are provided in Dataset S1.

To further investigate the concentration-dependent inhibition, we increased the interfacial surface area using the same mass of substrate in the reaction but in a powdered form produced by cryomilling the amorphous PET film. The micronization process has little effect on the amorphous nature of the PET substrate (Figure S9A); the cryomilled powder was found to have a comparably low crystallinity (10.4 ± 1.7%) to that of the original film (9.1 ± 1.9%). However, the powder has a surface area at least 7-times higher than the amorphous PET film (approximated from the particle dimension distributions obtained through dynamic image analysis; Figure S9B). As shown in Figure 4, the total aromatic product released from the amorphous powder increases with higher enzyme concentrations suggesting that an elevated surface area (and, hence, reduced enzyme loading per surface area) alleviates the concentration-dependent inhibition at the tested enzyme concentrations.

Enzyme concentration-dependent inhibition is common in mesophilic cutinases

To gain additional insight into the inhibition phenomenon, we investigated the enzyme concentration dependence on PET amorphous film hydrolysis with other type II enzymes from mesophilic hosts (Figure S10). We selected several *Is*PETase homologues from the type IIa and IIb (Tables S1–S3) including two enzymes from *Rhizobacter gummiphilus*, *Rg*Cut-I[5] and *Rg*Cut-II. The sequence identity of the selected enzymes with *Is*PETase varies from 51 to 82% (Table S3), and all exhibit absolute conservation of the catalytic triad residues and have a

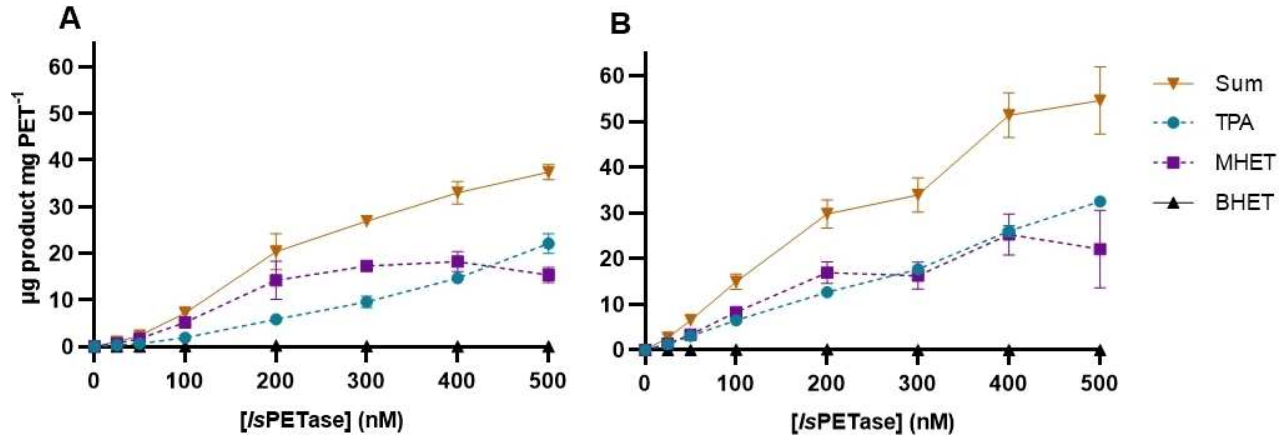

Figure 4. PET powder hydrolysis as a function of *Is*PETase concentration. Amorphous PET powder (characterization of which is shown in Figure S9) was incubated with different concentrations of *Is*PETase during 96 h at 30 °C in 50 mM KH_2PO_4/K_2HPO_4 at pH 8.0 (A) or bicine at pH 9.0 (B). PET powder was obtained by grinding PET amorphous film. Values for TPA (blue circles), MHET (purple squares), BHET (black triangles) and the sum of aromatic products (brown) are shown. Data are means ± SD of triplicate reactions. The data for these plots are in Dataset S1.

Trp residue in the X_1 position of the "lipase box" motif GX_1SX_2G. The highest activities for these enzymes were observed between pH 8.0 and 9.0, and at temperatures from 25 to 40 °C (Table S4) supporting identification of these enzymes as mesophilic. These enzymes have at least one order of magnitude lower PET-degrading activity than *Is*PETase, with *Rg*Cut-II exhibiting the highest activity among the homologues (Figure 5A). Each of these enzymes presented varying levels of concentration-dependent inhibition under their optimal solution conditions, with the exception of *Rg*Cut-II (Figure 5B, Figure S11), despite this enzyme belonging to the same type IIb group as *Is*PETase. There is no clear relationship between the extent of inhibition at high concentration and the phylogenetic grouping of the enzymes.

In addition, there is no correlation between the levels of PET hydrolysis and inhibition, suggesting that the phenomenon is not related to catalytic competence. With the exception of *Sb*Cut and *Rg*Cut-I, DMSO significantly increased the activity of the homologous enzymes, as observed with *Is*PETase (Figure 5A, Figure S12). Any relief of concentration-dependent inhibition offered by DMSO is also protein-dependent (Figure S13); reduction is seen for *Pa*Cut, *Sb*Cut, *Ad*Cut, and *Rg*Cut-I, but not for *Ps*Cut, *Pbauz*Cut or *Po*Cut.

In search of a structural basis

The variable susceptibilities of the type II enzymes to concentration-dependent inhibition suggests that this phenomenon could relate to enzyme structure and/or stability. Both experimental and computational structure models of these proteins were analyzed to look for protein characteristics associated with the inhibitory behavior. To this end, we solved the crystal structures of three enzymes – *Rg*Cut-II, *Ps*Cut and *Pbauz*Cut – to high resolution (Table S5). As expected, the structures were highly similar, with each conforming to the consensus α/β-hydrolase fold (Figure S14). However, structural features such as the width of the active site cleft (Figure S15) and the distribution of surface electrostatic charges (Figure S16) show no discernible correlation with the degree of concentration-dependent inhibition.

We next investigated the thermostability of the enzymes by measuring apparent melting temperature (T_m) values by differential scanning calorimetry (DSC). These mostly fell in the range of 48 to 52 °C (Table S6) with the exception of *Rg*Cut-II which has an apparent T_m of approximately 67 °C; this higher thermostability may reflect enhanced structural rigidity to the enzyme.

The multiple sequence alignment of the *Rg*Cut-II with the selected enzymes (Figure S17) reveals that *Rg*Cut-II has a shorter loop between $\beta 8$ and $\alpha 6$ – the length of which differentiates type II enzymes from type I – and which has been proposed to contribute in part to the binding of PET substrate.[4] To determine whether this loop influences the susceptibility to concentration-dependent inhibition, we constructed two mutants of *Is*PETase and *Rg*Cut-II in which the loop sequences (Ser242-Gly243-Asn244-Ser245-Asn246-Gln247-Ala248 and Asn234-Ala235-Asn236-Pro237, respectively) were interchanged. These were designed by alignment of the structures of *Is*PETase and *Rg*Cut-II taking into account the conservation of residues either side of the two loops. Verification by alignment of the *AlphaFold2*-predicted[29] structural models of the mutants suggested no evident extra structural changes introduced by the loop interchanges. However, DSC analyses indicated that the *Is*PETase^{Rg} (*Is*PETase with *Rg*Cut-II loop) and *Rg*Cut-II^{Is} (*Rg*Cut-II with *Is*PETase loop) variants were destabilized with respect to their wild-type counterparts by 4.4 and 7.5 °C, respectively (Table S6). Concentration-dependent inhibition was largely unaffected in the mutant *Is*PETase^{Rg} despite substantial

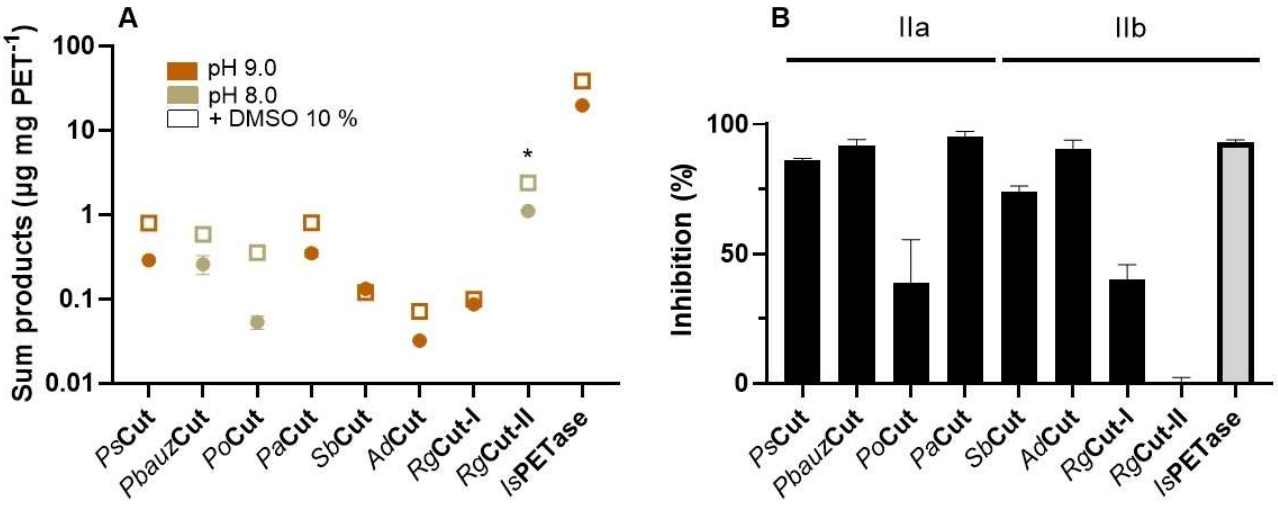

Figure 5. PET hydrolysis activity of mesophilic *Is*PETase homologues. (A) Comparative PET hydrolysis activity for each enzyme at their optimal pH in the absence or presence of 10% (v/v) DMSO. For each enzyme, reactions were performed at their optimal temperature (30 °C for all except *Rg*Cut-II, which was at 40 °C; marked by an asterisk). (B) The percentage of inhibition seen for each enzyme, calculated from the enzyme concentration-dependence PET hydrolysis data in Figure S11. Data are means ± SD of triplicate reactions. The assignments of enzymes to PET hydrolase groups IIa and IIb are depicted above the columns. The data for panels (A) and (B) are provided in Dataset S1.

loss of activity (Figure S18). In addition, only a small increase in inhibition was found with the *Rg*Cut-II^{ls} mutant (Figure S18) with a concomitant loss in activity. These results imply that there is no substantial effect of the extended β8-α6 loop on the susceptibility of *Is*PETase to concentration-dependent inhibition.

We undertook a detailed comparison of *Rg*Cut-II and *Is*PETase, with a particular focus on internal structural details. We note that *Is*PETase has several previously unappreciated internal cavities that may influence in the rigidity of the active site of the enzyme allowing residues mobilities (Figure 6). Adjacent to the active site of *Is*PETase, as well as all the analyzed mesophilic enzymes, a cavity exists between Ala240 and Ile250 that is substantially filled in *Rg*Cut-II by the bulkier residues phenylalanine (Phe232) and valine (Val239; Figure 6). Filling this cavity could reduce flexibility of the active site.

To test this hypothesis, we made the *Rg*Cut-II F232A/V239I variant and investigated its susceptibility to inhibition at high concentration (Figure 6C). This variant exhibited a similar melting temperature to the wild-type *Rg*Cut-II enzyme (Table S6). Although modest, an increase in concentration-dependent inhibition from 0 to 31% at 40 °C was found, suggesting an inverse relationship between active site rigidity and inhibition susceptibility.

Concentration-dependent inhibition can be reduced by enzyme engineering

It has been noted that the residues that surround the *Is*PETase active site differ from those of thermotolerant PET hydrolases.[4] In prior work, it was shown that interchanging two residues at the active site (W159H/S238F)[30] enhances the melting temperature of *Is*PETase by 10 °C, and its activity at elevated temperatures.[16] Here, we found that this double mutant also shows reduced susceptibility to inhibition at high concentration compared to the wild-type enzyme at both pH 8.0 and pH 9.0 (Figure 7). It is noteworthy that the residue Ser238 variation to phenylalanine or tyrosine is common amongst the type II enzymes (Figure S17, Figure S19), including *Rg*Cut-II (Phe230), with no evident effect on inhibition, suggesting that the double mutant needs both substitutions to affect its increased thermal stability and reduced susceptibility to inhibition. From a structural point of view, this combination of mutations may stabilize the loop structure where the active site histidine (His237) is located, reducing its flexibility.

Inhibition is eliminated in HotPETase

Since, for the *Is*PETase W159H/S238F variant, a gain in thermostability accompanies a decrease in concentration-dependent inhibition, we investigated the phenomenon in two other, previously reported, thermostable variants, *Is*PETase$^{S121E/D186H/R280A}$[31] and HotPETase.[3] The latter has multiple mutations and exhibits a dramatic increase in thermostability with an apparent T_m of 83.8 °C under our measurement conditions (Table S6) and an optimal activity temperature of 65 °C. However, HotPETase has the unusual property of maintaining the same activity as the wild-type enzyme at lower temperature[3] which allows for comparison of any concentration-dependent inhibition under the same conditions. Compared to the wild-type IsPETase, the inhibition in *Is*PETase$^{S121E/D186H/R280A}$ is greatly reduced at 30 °C (Figure 8A), minimal at 40 °C (Figure S20A), and abolished at 50 °C (Figure S20B), although PET hydrolysis activity is drastically lower at this highest temperature. Similarly, concentration-dependent inhibition is totally absent in HotPETase at 30 °C (Figure 8A), corroborating the observation that increased thermostability is often correlated with reduced inhibition. Analysis of the HotPETase structure indicates that the number of cavities is reduced in this enzyme including in the region of the active site (Figure S21). Finally, comparative molecular dynamics simulations of wild-type IsPETase and HotPETase reveal that HotPETase has significantly less flexibility in the vicinity of the active site (Figure 8B, Figure S22), further supporting the association of concentration-dependent inhibition with active site flexibility.

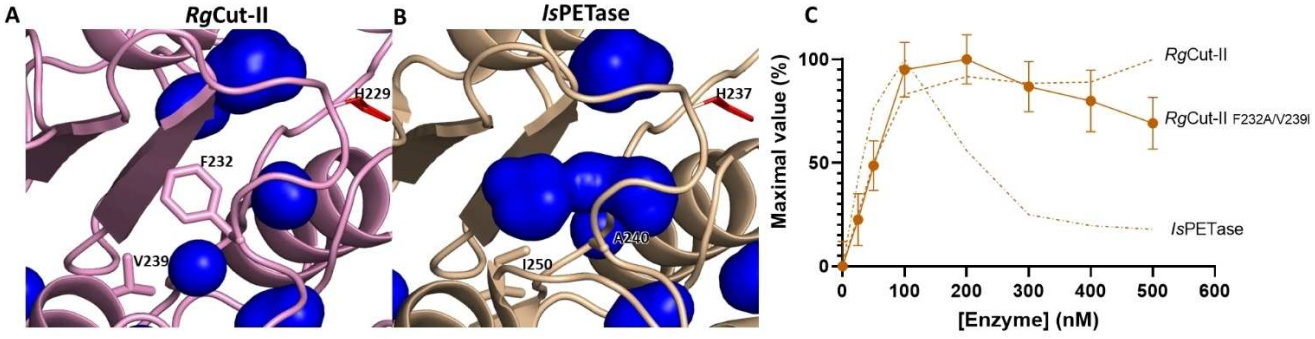

Figure 6. Structural and functional comparison of *Rg*Cut-II with *Is*PETase. (A,B) Structural cavities in the proximity of the active site for (A) *Rg*Cut-II (PDB: 8AIR) and (B) *Is*PETase (PDB: 6EQE) are shown as blue clouds. A cavity present in *Is*PETase is partially occupied by residues Phe232 and Val239 in *Rg*Cut-II. The sidechain of the catalytic triad histidine (H) is shown in red. (C) PET film hydrolysis (% of maximal value) as a function of the enzyme concentration for *Rg*Cut-II, *Rg*Cut-II F232 A/V239I variant and *Is*PETase. Amorphous PET film coupons were incubated with different concentrations of the enzyme for 96 h at 40 °C in bicine buffer at pH 9.0. Values for the sum of aromatic products are shown. The highest activity in each case was set to 100%. For comparison the profiles for *Is*PETase and *Rg*Cut-II are included. Error bars represent SD of reactions of triplicate reactions. The dataset for this plot is in Dataset S1.

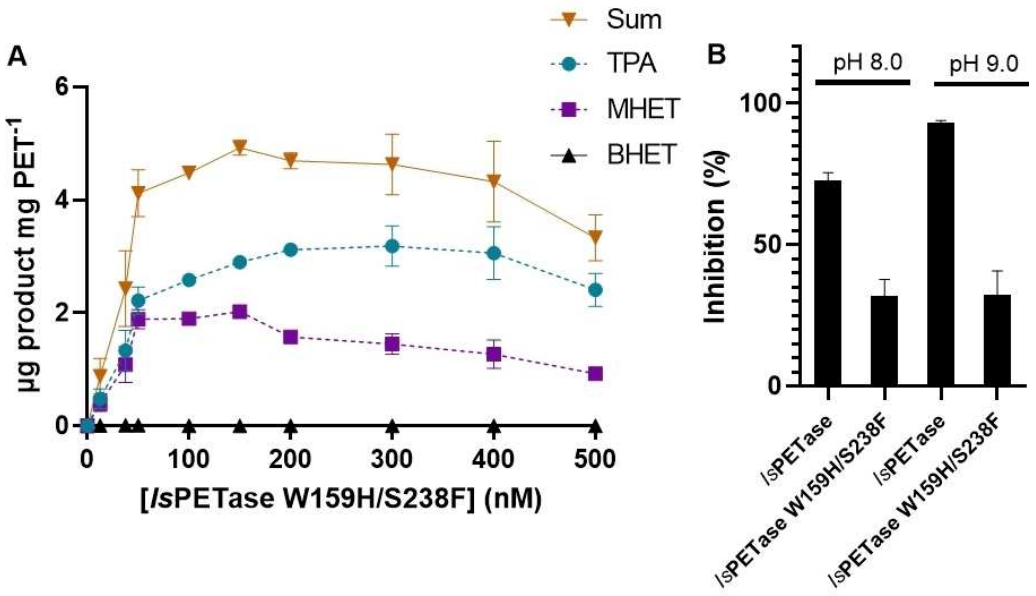

Figure 7. Reduction of concentration-dependent inhibition in the engineered *Is*PETase (W159H/S238F) variant. (**A**) PET film hydrolysis as a function of *Is*PETase W159H/S238F concentration. Amorphous PET films were incubated with different concentrations of the enzyme for 96 h at 30 °C in bicine buffer at pH 9.0. Values for TPA (blue), MHET (purple), BHET (black) and the sum of aromatic products (brown) are shown. Data are means ± SD of triplicate reactions. (**B**) Comparison of inhibition levels at 500 nM enzyme concentration between *Is*PETase and the *Is*PETase W159H/S238F variant at pH 8.0 and pH 9.0. Data for these plots are in Dataset S1.

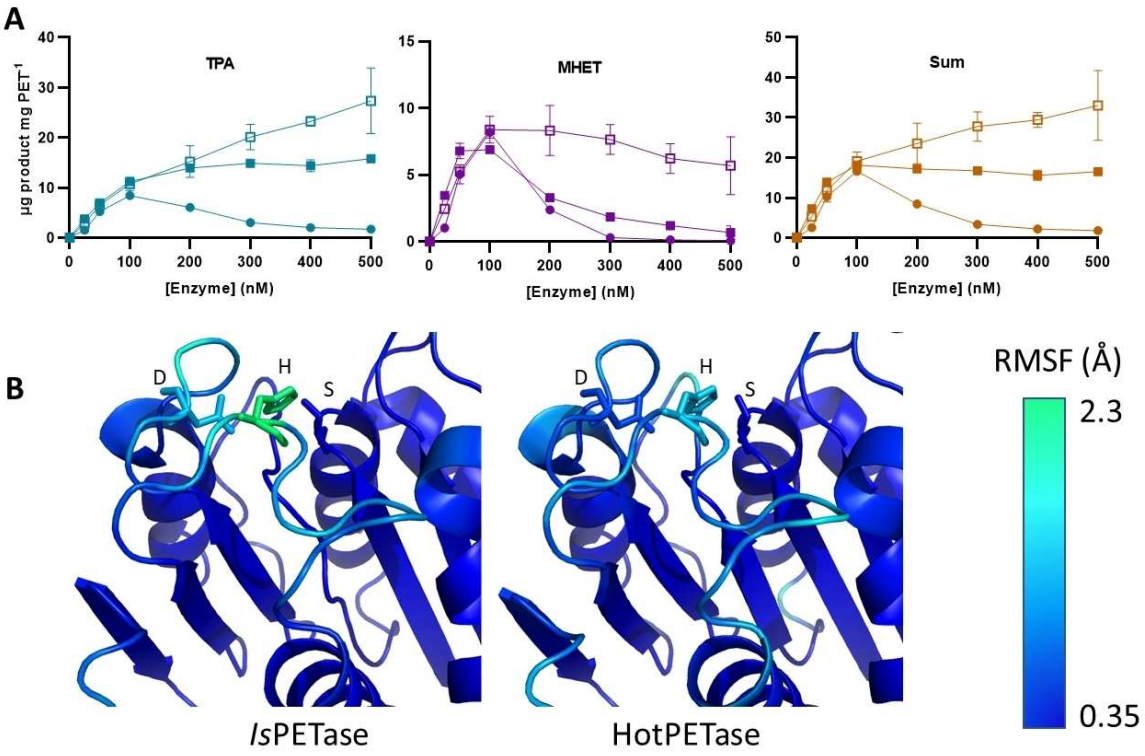

Figure 8. Comparison of concentration-dependent inhibition between *Is*PETase and HotPETase. (A) PET film hydrolysis as a function of the enzyme concentration for *Is*PETase (solid circle), *Is*PETase$^{S121E/D186H/R280A}$ (solid square) and HotPETase (open square). Amorphous PET films were incubated with the specified enzyme concentration for 96 h at 30 °C in bicine buffer pH 9.0. Blue, purple, and brown represent the values obtained for TPA, MHET and the sum of the aromatic products, respectively. Data are means ± SD of triplicate reactions. (B) The crystal structures of IsPETase and HotPETase are shown with residues colored (scale on right) according to the backbone root mean square fluctuations (RMSF) from the molecular dynamics simulations. The catalytic triad Ser160, Asp206 and His237 are shown. The dataset for this plot is in Dataset S1.

Discussion

Enzymes working at surfaces, such as in plastic biodegradation, contend with challenges not observed in solution, for example, strong orientational effects and high local enzyme concentrations. In such interfacial catalysis, the reaction rate is hyperbolic with respect to enzyme concentration, due to the saturation of accessible scissile bonds on the substrate.[15,17] In contrast to this, here we have shown that for *Is*PETase and numerous mesophilic homologues, the extent of reaction is not hyperbolic in profile; instead, it reaches a maximum then falls as the enzyme concentration rises.[2,15,20]

In this study, we analyzed concentration-dependent inhibition in multiple natural *Is*PETase homologues and engineered variants of *Is*PETase itself, and we demonstrated that the extent of inhibition on PET is related to the dynamic properties of the enzyme, including regions around the active site; less thermostable enzymes are often more susceptible to inhibition at high enzyme concentration. For each enzyme, the extent of inhibition depends on temperature, solution conditions (pH and the concentration of DMSO), and substrate surface area. The influence of these parameters can explain the different results obtained previously for the enzyme concentration dependence of *Is*PETase in different studies.[2,16,20] However, a molecular explanation for these observations is beyond the scope of this work; it will require future developments in our collective understanding of enzymatic properties at the solid-liquid interface and how these influence PET depolymerization performance.

A previous study of the surface adsorption to PET particles by PET-degrading enzymes including *Is*PETase, showed a strong adsorption[32] (with a K_d for *Is*PETase of 22 nM), with a concomitant formation of an enzyme monolayer when the substrate surface is saturated. In our study, concentration-dependent inhibition occurs at concentrations above 50–100 nM enzyme with the PET films. Given the dimensions of our stadium-shaped PET film coupons (13×3×0.25 mm), and a calculated footprint of *Is*PETase on PET particles (9 nm^2),[32] we can estimate a maximal surface coverage of 1.42 nmol g^{-1} PET, equivalent to around 15 pmol per film piece. With these parameters, the mole fraction of bound enzyme at maximal activity, calculated as described previously,[32] could be estimated to 0.23 with an occupancy of 11.7 pmol per film piece at 100 nM, close to the monolayer limit of 15. This occupancy value indicates a high coverage for *Is*PETase on the film for the enzyme concentrations at which inhibition is evident.

The fact that concentration-dependent inhibition is witnessed on PET film but not on PET powder (of an equivalent mass) is an argument against the possibility of aggregation-mediated enzyme inactivation in bulk solution or a reduction in available substrate scissile bonds by enzyme hydrolysis. Moreover, the appearance of concentration-dependent inhibition at high enzyme coverage is consistent with an inhibitory surface crowding effect as described previously.[15,16] Under crowding conditions, lateral enzyme–enzyme interactions could potentially interfere with enzyme-substrate binding. For example, they may change the enzyme orientation with respect to the plastic surface leading to binding at unproductive sites on the enzyme. Alternatively, crowding could elicit conformational changes in the enzyme exposing unproductive binding sites resulting in surface capture of enzyme molecules in inactive orientations. In support of this, overshooting adsorption – where adherence to a hydrophobic surface is enhanced compared to the simple adsorption-desorption Langmuir model – has been associated with a high bulk protein concentration, and explained by an alteration, over time, in the orientation of protein absorbed on the surface.[33]

It is noticeable in our results that concentration-dependent inhibition of *Is*PETase is greater at pH 9.0 than pH 8.0. Since pH 9.0 is closer to the enzyme's pI (9.65), a reduction in electrostatic repulsion between enzyme molecules could allow for greater packing densities on the surface,[33] thus exacerbating any inhibitory effects. Similarly, DMSO may relieve inhibitory enzyme–enzyme hydrophobic interactions at the plastic surface. In fact, DMSO can change several properties of proteins including their binding capacity.[34] Furthermore, the effect of DMSO is known to be protein-dependent[35] explaining its varied influence on activity and enzyme concentration-dependent inhibition among the studied mesophilic enzymes.

Although not apparent with the first 30 min of incubation, the inhibition accumulates rapidly during the following few hours. This temporal dependence could be explained by a time-dependent accumulation of non-productively bound enzyme, as described in the above overshooting absorption kinetic model.[33] In addition, the lack of concentration-dependent inhibition during the initial incubation phase could be due to the early release of PET fragments (soluble or insoluble) by endo-type cleavage[36,37] which may recruit and sequester enzyme molecules thus decreasing the initial rate of surface deposition. Whilst it is possible that the product inhibition that has been reported for other PET degrading enzymes[8] could play a role in concentration-dependent inhibition, this seems unlikely as the phenomenon is evident well before significant concentrations of any monomeric products can accumulate.

It is conceivable that crowding-induced changes in enzyme conformation – and, hence, a reduction in PET degrading activity – would be exacerbated for enzymes of lower structural rigidity. Indeed, previous molecular dynamic simulations revealed greater mobility in the active site of *Is*PETase than thermophilic enzymes like LCC and TfCut2;[38] in general, unlike *Is*PETase, such thermophilic enzymes do not exhibit concentration-dependent inhibition at their optimal temperatures.[15] This contrast in behaviors could arise both from differences in enzyme biophysical properties, and from differential substrate accessibility at the enzymes' optimal temperatures. However, the contribution of the latter factor might seem less important because those surface polymer chains in the vicinity of the bulk solvent (and, hence, most susceptible to enzymatic hydrolysis) already have a considerably lower glass transition temperature (T_g = 40–48 °C) compared to those buried within the bulk material (T_g = 65–71 °C);[8,37] this difference is due to an intrinsically lower degree of order near the polymer surface, compounded by plasticization due to water ingress.[8] However, the observed alleviation of *Is*PETase$^{S121E/D186H/R280A}$ concentration-

dependent inhibition when the temperature is increase from 30 °C to 50 °C, suggests that substrate mobility does influence the phenomenon.

Although it is not always the case, protein mobility can be reduced when thermostability is increased.[39] Here, the association of greater thermostability with reduced inhibition at high enzyme concentration supports the notion that elevated active site flexibility favors unproductive binding to the polymer. *Rg*Cut-II, the most thermostable of the analyzed wild-type enzymes, lacks any such inhibition despite reaching maximal activity at around 100 nM enzyme concentration. This is likely reflective of a diminished active site flexibility associated with the increased thermal tolerance, which is supported by a reduction in the size of a cavity near the catalytic site. In addition, the mutants of *Is*PETase, W159H/S238F and S121E/D186H/R280 A, which have around a 10 °C higher apparent T_m than the wild-type enzyme, exhibit substantially reduced inhibition compared to the wild-type enzyme. Similarly, concentration-dependent inhibition is absent in the thermostable mutant HotPETase which has a less flexible active site than wild-type IsPETase.

The results shown here indicate that inhibition of mesophilic PET-hydrolyzing enzymes at high concentration can be mitigated, and even avoided, by increasing the substrate surface area, for example, by cryomilling; however, this requires a significant input of energy that would negatively impact both the economics and carbon footprint of enzymatic PET recycling.[26,27] Alternatively, we propose that increased rigidity can be productively engineered into the mesophilic enzymes that exhibit this behavior. In addition, the identification and elimination of any unproductive binding sites could help in the development of enzymes that are resistant to inhibition at high concentration.

Conclusion

The inhibition of *Is*PETase and its mesophilic homologues at high enzyme concentration is an obstacle to the industrial use of these natural enzymes. This impediment can be partially resolved by adding an organic cosolvent (in this case, DMSO), or increasing the substrate surface area by cryomilling. Alternatively, enzyme engineering can be employed to enhance enzyme thermostability to reduce or even eliminate concentration-dependent inhibition. These two strategies can minimize the negative impact of enzyme–enzyme interactions on a densely populated PET surface.

Experimental Section

Substrates and products

Bis(hydroxyethyl) terephthalate (BHET) and terephthalic acid (TPA) were purchased from Sigma-Aldrich. Mono-(2-hydroxyethyl)terephthalic acid (MHET) was synthesized and supplied by ChiroBlock GmbH (Germany). Amorphous, 0.25 mm-thick PET film sheet was supplied by Goodfellow (product number ES30-FM-000145). In preparation for enzyme hydrolysis assays, 10.5 mg stadium shaped pieces with dimensions 13×3×0.25 mm were prepared from the PET film sheet using a hole punch. A micronized amorphous powder was produced from this PET film by cryomilling, first in a SM300 cutting mill (Retsch), then in a ZM200 centrifugal mill (Retsch), as described previously.[40] After air drying, the particle size and shape distributions in the PET powder were assessed by dynamic image analysis using a CAMSIZER X2 (Microtrac MRB) with X-Fall module. Thereafter, an approximation of the powder surface area was calculated from the derived distributions of particle cross-sectional area and aspect ratio. Quantitative analysis of the PET crystallinity was performed by DSC using a DSC 214 *Polyma* (Netzsch) both before and after cryo-milling.

Plasmid construction

Nucleotide and amino acid sequences, Genbank accession numbers and organism sources of the enzymes used in this study are shown in the Tables S1–S3. Amino acid sequences with homology to *Is*PETase and belonging to the Type IIa and IIb groups of the PET-degrading enzymes, were retrieved from NCBI database using protein BLAST software. These sequences were codon optimized for expression in *E. coli* K12 MG1655 (Highly Expressed Genes) using the codon optimizer at http://genomes.urv.es/OPTIMIZER/ (guided random method).[41] The sequences included the signal peptide predicted by Signal 6 software.[41] The stop codon was omitted and overlaps were added for assembly into the expression vector pET-21b(+) such that the assembly would results in the addition of a C-terminal 6 His tag. These sequences were synthesized as linear DNA fragments by IDT and assembled using NEBuilder® HiFi DNA Assembly Master Mix (New England Biolabs) according to the manufacturer's instructions into pET-21b(+) digested with NdeI and XhoI. *Is*PETase[2] and the double mutant of *Is*PETase W159H/S238F,[30] have been described elsewhere. Mutants of *Rhizobacter gummiphilus* cutinase II (*Rg*Cut-II) and other mutants of *Is*PETase were assembled in pET-29. The HotPETase[3] gene and the *Is*PETase variant (*Is*PETase S121E/D186E/R280 A),[31] cloned in the expression plasmid pBbE8 K, was kindly provided by Anthony Green, University of Manchester.

Recombinant expression of enzymes

Enzyme expression plasmids were transformed into BL21-C41 (DE3) *E. coli* cells (Sigma), with the exception of HotPETase and the IsPETase S121E/D186E/R280 A which were expressed in T7-SHuffle *E. coli* cells (NEB). Isolated colonies from the transformation plates were inoculated into antibiotic-containing liquid medium, either a non-inducing minimum medium containing glucose[42] for subsequent autoinduction expression, or 2YT medium; these starter cultures were grown overnight at 37 °C with shaking. The starter cultures were used to inoculate multiple 500 mL cultures of either 2YT broth or ZYM-5052 auto-induction medium[42] (Table S7) in 2 L Erlenmeyer flasks (total volume between 2 and 4 L for each enzyme); these were then incubated in an Eppendorf shaking incubator at 160 rpm at 37 °C. For cells grown in 2YT medium, the culture was grown to an OD_{600} of 0.6, induced by adding either arabinose to 10 mM (for HotPETase and the *Is*PETase variant S121E/D186E/R280 A) or IPTG to 1 mM (all other enzymes), and returned to the incubator for 18 h at 20 °C. For the auto-inductive expression in ZYM-5052, the cells were grown at 28 °C for 28 h. In each case, cells were harvested by centrifugation and the pellet stored at −20 °C prior to purification.

Enzyme purification

Pellets from 1 L cultures were resuspended in 50 mL lysis buffer (20 mM Tris pH 8, 300 mM NaCl, 10 mM imidazole) in the presence of DNAse and lysed by sonication (40% power, 3 s on, 9 s off for a total of 5 min). The lysate was centrifuged at 40,000 g X 30 min at 4 °C, and the supernatant purified by affinity chromatography at 4 °C on a 5 mL HisTrap HP column (Cytiva) pre-equilibrated with lysis buffer. After washing, the enzyme was eluted with a linear gradient of 10 to 250 mM imidazole over 120 mL. Fractions containing the protein of interest were identified by SDS-PAGE and concentrated to 5 mL by ultrafiltration using Amicon Ultra-15 (Sigma) with 10 kDa MW cut-off and loaded at 4 °C onto a HiLoad 16/600 Superdex 200 (Cytiva) size exclusion column that had been pre-equilibrated with Tris 20 mM pH 8, 0.3 M NaCl. The purity and molecular weight of the eluted proteins were assessed by SDS-PAGE with Coomassie staining, and the protein of interest was identified by Western blotting using an anti-His-tag monoclonal antibody (Invitrogen), a horseradish peroxidase coupled anti-mouse IgG conjugate (Sigma), with visualization using the enhanced chemiluminescence method (ECL substrates, GE Healthcare). The purified proteins were concentrated and dialyzed in Tris 20 M, pH 8, 100 mM NaCl using a PD 10 column and stored at −20 °C with 10% glycerol.

Enzyme differential scanning calorimetry

For those enzymes that were purified to a high enough yield, an apparent melting temperature (T_m) was determined by DSC on a MicroCal PEAQ-DSC Automated instrument (Malvern Panalytical). Previous analysis, the samples were submitted to size exclusion chromatography in a HiLoad Superdex 75 pg column (Cytiva) equilibrated in 50 mM NaH_2PO_4/Na_2HPO_4, 100 mM NaCl pH 7.5. DSC analyses were performed in triplicate using 0.2 mg mL^{-1} and the temperature of the sample was raised from 30 °C to 120 °C at 1.5 °C min^{-1}. Buffer subtraction, baseline correction and apparent T_m determination were performed using the instrument's control and analysis software.

Structure determination and modelling of IsPETase homologues

The structures of *Is*PETase (PDB: 6EQE), double mutant *Is*PETase (W159H/S238F; PDB: 7OSB) and HotPETase (PDB: 7QVH) have been described previously. For crystallization of *Rg*Cut-II, *Ps*Cut and *Pbauz*Cut, each protein was concentrated to 10 mg mL^{-1} and sitting drop crystallization trials were set up using a Honeybee X8 robot (Genomic Solutions). Protein crystals appeared in the following screens and conditions: *Rg*Cut-II – Proplex screen (Molecular Dimensions), G11, 0.1 M HEPES pH 7.5, 1 M sodium acetate; *Ps*Cut – JCSG-plus screen (Molecular Dimensions), B7, 0.1 M sodium acetate pH 4.6, 8% PEG 4000; *Pbauz*Cut – JCSG-plus screen (Molecular Dimensions), A1, 0.1 M sodium acetate pH 4.5, 0.2 M lithium sulfate, 50% PEG 400. Diffraction data were collected at the Diamond Light Source (Didcot, UK) and processed using DIALS[43,44] on ISPyB. The structure was solved by molecular replacement with MOLREP[45] using structure homologs. Model buildings were performed in Coot[46] and the structures were refined with REFMAC5.[47] MolProbity[48] was used to evaluate the final structure models. Data and Refinement statistics are summarized in Table S5. The atomic coordinates have been deposited in the Protein Data Bank and are available under the accession codes 8AIR, 8AIS and 8AIT. The structures of another *Is*PETase homologue were predicted using Alphafold2[29] with the default parameters. All enzyme structures were visualized in PyMOL (Schrödinger, LLC).

Molecular dynamics simulations

Molecular dynamics simulations of *Is*PETase and HotPETase were performed with the AMBER20 package[49] and the CHARMM forcefield.[50] The structures of the proteins were prepared with CHARMM-GUI.[51] The proteins were surrounded with 12 Å of water and 0.1 M of potassium chloride in a cubic box. Langevin dynamics were performed with a time step of 2 fs using SHAKE,[52] a friction coefficient of 1 ps^{-1}, and a temperature of 300 K. The cutoff was 12 Å using force-switching with a switching region of 2 Å.[53] Electrostatic interactions were treated with the Particle Mesh Ewald method.[54] After an equilibration of 50 ns at 1 atm, the root mean square fluctuations of the protein backbone were determined during 150 ns of production. The trajectories were processed with cpptraj[53,55] and analyzed with the CHARMM program.[56]

Biochemical assays on PET film

Enzymatic reactions (500 μL) were performed in triplicate in propylene tubes (Sarted), containing either 50 mM KH_2PO_4/K_2HPO_4 pH 8.0 or 50 mM bicine pH 9.0, and enzyme at different concentrations (up to 500 nM) except when evaluating the effect of different PET loadings, when up to 4 μM enzyme was used. Where indicated for some experiments, DMSO was added in the reaction at 10% (v/v) final concentration. Unless specified otherwise, the samples were incubated for 96 h at 30 °C. A sample with PET without enzyme was used as a blank. To stop the reaction, the PET was removed, the solution incubated at 90 °C for 10 min and centrifugated at 15,000 g for 10 min. The released products from the enzymatic reaction, TPA, MHET and BHET were quantified using an Agilent 1260 high pressure liquid chromatography (HPLC) system equipped with diode array detector at a wavelength of 240 nm and using a Phenomenex Luna C18 column, 5 μm, 4.6× 150 mm as described previously.[16] A calibration curve was performed with each analyte with concentrations between 3 and 100 ng μL^{-1} and analyzed with the same conditions than the samples.

Biochemical assays using monomer substrates

For determination of MHET and BHET hydrolysis rates, reactions were performed in triplicate using 2 mM substrate and 100 nM (for MHET hydrolysis) or 10 nM (for BHET hydrolysis) of *Is*PETase concentration in a reaction comprising 98% (v/v) 50 mM KH_2PO_4/K_2HPO_4 pH 8.0, 2% (v/v) DMSO, at 30 °C. BHET and MHET were solubilized in 100% (v/v) DMSO before addition to the reaction mixture. Reactions were terminated using an equal volume of 100% methanol. Product and substrate were quantified by HPLC. The apparent turnover rate (k_{cat}) was calculated using either the concentration of TPA produced in the case of MHET hydrolysis, or the sum of MHET and TPA produced in the case of BHET hydrolysis.

Acknowledgements

We thank Anthony Green and Elizabeth Bell for providing the plasmid for HotPETase. JEM, ARP, LA, BRL, GK, MZ, LO, MC and VB thank Research England for E3 funding. JEM thanks the BBSRC for grant BB/P011918/1. RG was funded through an NREL subcontract and University of Portsmouth Faculty of Science bursary. This work was authored in part by Alliance for Sustainable Energy, LLC, the manager and operator of the National Renewable Energy Laboratory (NREL) for the U.S. Department of Energy (DOE) under

Contract No. DE-AC36-08GO28308. Funding was provided by the U.S. DOE, Office of Energy Efficiency and Renewable Energy, Advanced Manufacturing Office (AMO) and Bioenergy Technologies Office (BETO). This work was performed as part of the Bio-Optimized Technologies to keep Thermoplastics out of Landfills and the Environment (BOTTLE) Consortium and was supported by AMO and BETO under contract no. DE-AC36-08GO28308 with NREL, operated by Alliance for Sustainable Energy, LLC. The BOTTLE Consortium includes members from the University of Portsmouth, funded under contract no. DE-AC36-08GO28308 with NREL. The views expressed in the article do not necessarily represent the views of the DOE or the U.S. Government. The U.S. Government retains and the publisher, by accepting the article for publication, acknowledges that the U.S. Government retains a nonexclusive, paid-up, irrevocable, worldwide license to publish or reproduce the published form of this work, or allow others to do so, for U.S. Government purposes. We thank staff at the Diamond Light Source for beamtime and support. We would also like to thank Daniel Hinchen and Tom Shakespeare for helpful conversations in support of this work.

Conflict of Interest

The authors declare no conflict of interest.

Data Availability Statement

The data that support the findings of this study are available in the supplementary material of this article.

Keywords: biocatalysis · hydrolases · mesophilic enzymes · PETase · plastics

[1] F. Kawai, T. Kawabata, M. Oda, *Appl. Microbiol. Biotechnol.* **2019**, *103*, 4253.
[2] S. Yoshida, K. Hiraga, T. Takehana, I. Taniguchi, H. Yamaji, Y. Maeda, K. Toyohara, K. Miyamoto, Y. Kimura, K. Oda, *Science* **2016**, *351*, 1196.
[3] E. L. Bell, R. Smithson, S. Kilbride, J. Foster, F. J. Hardy, S. Ramachandran, A. A. Tedstone, S. J. Haigh, A. A. Garforth, P. J. R. Day, C. Levy, M. P. Shaver, A. P. Green, *Nat. Catal.* **2022**, *5*, 673–681.
[4] S. Joo, I. J. Cho, H. Seo, H. F. Son, H. Y. Sagong, T. J. Shin, S. Y. Choi, S. Y. Lee, K. J. Kim, *Nat. Commun.* **2018**, *9*, 382.
[5] H. Y. Sagong, H. F. Son, H. Seo, H. Hong, D. Lee, K. J. Kim, *J. Hazard. Mater.* **2021**, *416*, 126075.
[6] C. C. Chen, X. Han, X. Li, P. Jiang, D. Niu, L. Ma, W. Liu, S. Li, Y. Qu, H. Hu, J. Min, Y. Yang, L. Zhang, W. Zeng, J.-W. Huang, L. Dai, R.-T. Guo, *Nat. Catal.* **2021**, *4*, 425–430.
[7] F. Kawai, T. Kawabata, M. Oda, *ACS Sustainable Chem. Eng.* **2020**, *8*, 8894–8908.
[8] R. Wei, G. von Haugwitz, L. Pfaff, J. Mican, C. P. S. Badenhorst, W. Liu, G. Weber, H. P. Austin, D. Bednar, J. Damborsky, U. T. Bornscheuer, *ACS Catal.* **2022**, *12*, 3382–3396.
[9] A. K. Herzog, R. J. Müller, W. D. Deckwer, *Polym. Degrad. Stab.* **2006**, *91*, 2486.
[10] Å. M. Ronkvist, W. Xie, W. Lu, R. A. Gross, *Macromolecules* **2009**, *42*, 5128–5138.
[11] R. Wei, T. Oeser, M. Barth, N. Weigl, A. Lübs, M. Schulz-Siegmund, M. C. Hacker, W. Zimmermann, *J. Mol. Catal. B* **2014**, *103*, 72–78.
[12] K. Vogel, R. Wei, L. Pfaff, D. Breite, H. Al-Fathi, C. Ortmann, I. Estrela-Lopis, T. Venus, A. Schulze, H. Harms, U. T. Bornscheuer, T. Maskow, *Sci. Total Environ.* **2021**, *773*, 145111.
[13] E. L. Pfaff, J. Gao, Z. Li, A. Jäckering, G. Weber, J. Mican, Y. Chen, W. Dong, X. Han, C. G. Feiler, Y.-F. Ao, C. P. S. Badenhorst, D. Bednar, G. J. Palm, M. Lammers, J. Damborsky, B. Strodel, W. Liu, U. T. Bornscheuer, R. Wei, *ACS Catal.* **2022**, *12*, 9790–9800.
[14] R. Wei, T. Oeser, J. Then, N. Kuhn, M. Barth, J. Schmidt, W. Zimmermann, *AMB Express* **2014**, *4*, 44.
[15] J. Arnling Bååth, K. Borch, K. Jensen, J. Brask, P. Westh, *ChemBioChem* **2021**, *22*, 1627–1637.
[16] E. Erickson, T. J. Shakespeare, F. Bratti, B. L. Buss, R. Graham, M. A. Hawkins, G. König, W. E. Michener, J. Miscall, K. J. Ramirez, N. A. Rorrer, M. Zahn, A. R. Pickford, J. E. McGeehan, G. T. Beckham, *ChemSusChem* **2022**, *15*, e202102517.
[17] J. Arnling Bååth, K. Jensen, K. Borch, P. Westh, J. Kari, *JACS Au* **2022**, *2*, 1223–1231.
[18] J. Kari, M. Andersen, K. Borch, P. Westh, *ACS Catal.* **2017**, *7*, 4904–4914.
[19] J. Kari, S. J. Christensen, M. Andersen, S. S. Baiget, K. Borch, P. Westh, *Anal. Biochem.* **2019**, *586*, 113411.
[20] E. Z. L. Zhong-Johnson, C. A. Voigt, A. J. Sinskey, *Sci. Rep.* **2021**, *11*, 928.
[21] K. Mukai, K. Yamada, Y. Doi, *Int. J. Biol. Macromol.* **1993**, *15*, 361–366.
[22] M. Scandola, M. L. Focarete, G. Frisoni, *Macromolecules* **1998**, *31*, 3846–3851.
[23] S. Nayak, W.-S. Yeo, M. Mrksich, *Langmuir* **2007**, *23*, 5578–5583.
[24] B. C. Knott, E. Erickson, M. D. Allen, J. E. Gado, R. Graham, F. L. Kearns, I. Pardo, E. Topuzlu, J. J. Anderson, H. P. Austin, G. Dominick, C. W. Johnson, N. A. Rorrer, C. J. Szostkiewicz, V. Copié, C. M. Payne, H. L. Woodcock, B. S. Donohoe, G. T. Beckham, J. E. McGeehan, *Proc. Natl. Acad. Sci. USA* **2020**, *117*, 25476–25485.
[25] S. Brott, L. Pfaff, J. Schuricht, J. N. Schwarz, D. Böttcher, C. P. S. Badenhorst, R. Wei, U. T. Bornscheuer, *Eng. Life Sci.* **022**, *22*, 192–203.
[26] A. A. Singh, N. A. Rorrer, S. R. Nicholson, E. Erickson, J. S. DesVeaux, A. F. T. Avelino, P. Lamers, A. Bhatt, Y. Zhang, G. Avery, L. Tao, A. R. Pickford, A. C. Carpenter, J. E. McGeehan, G. T. Beckham, *Joule* **2021**, *5*, 2479–2503.
[27] B. T. Uekert, J. S. DesVeaux, A. Singh, S. R. Nicholson, P. Lamers, T. Ghosh, J. E. McGeehan, A. C. Carpenter, G. T. Beckham, *Green Chem.* **2022**, *24*, 6531–6543.
[28] R. Graham, E. Erickson, R. K. Brizendine, D. Salvachúa, W. E. Michener, Y. Li, Z. Tan, G. T. Beckham, J. E. McGeehan, A. R. Pickford, *Chem. Catal.* **2022**, *2*, 2644–2657.
[29] J. Jumper, R. Evans, A. Pritzel, T. Green, M. Figurnov, O. Ronneberger, K. Tunyasuvunakool, R. Bates, A. Žídek, A. Potapenko, A. Bridgland, C. Meyer, S. A. A. Kohl, A. J. Ballard, A. Cowie, B. Romera-Paredes, S. Nikolov, R. Jain, J. Adler, T. Back, S. Petersen, D. Reiman, E. Clancy, M. Zielinski, M. Steinegger, M. Pacholska, T. Berghammer, S. Bodenstein, D. Silver, O. Vinyals, A. W. Senior, K. Kavukcuoglu, P. Kohli, D. Hassabis, *Nature* **2021**, *596*, 583–589.
[30] H. P. Austin, M. D. Allen, B. S. Donohoe, N. A. Rorrer, F. L. Kearns, R. L. Silveira, B. C. Pollard, G. Dominick, R. Duman, K. El Omari, V. Mykhaylyk, A. Wagner, W. E. Michener, A. Amore, M. S. Skaf, M. F. Crowley, A. W. Thorne, C. W. Johnson, H. L. Woodcock, J. E. McGeehan, G. T. Beckham, *Proc. Natl. Acad. Sci. USA* **2018**, *115*, E4350.
[31] H. F. Son, I. J. Cho, S. Joo, H. Seo, H. Sagong, S. Y. Choi, S. Y. Lee, K. Kim, *ACS Catal.* **2019**, *9*, 3519.
[32] S. F. Badino, J. A. Bååth, K. Borch, K. Jensen, P. Westh, *Enzym. Microb. Technol.* **2021**, *152*, 109937.
[33] M. Rabe, D. Verdes, S. Seeger, *Adv. Colloid Interface Sci.* **2011**, *162*, 87–106.
[34] A. Tjernberg, N. Markova, W. J. Griffiths, D. Hallén, *J. Biomol. Screen* **2006**, *11*, 131–137.
[35] D. S. H. Chan, M. E. Kavanagh, K. J. McLean, A. W. Munro, D. Matak-Vinković, A. G. Coyne, C. Abell, *Anal. Chem.* **2017**, *89*, 9976–9983.
[36] A. S. Schubert, K. Schaller, J. A. Bååth, C. Hunt, K. Borch, K. Jensen, J. Brask, P. Westh, *ChemBioChem* **2022**, *24*, e202200516.
[37] N. A. Tarazona, R. Wei, S. Brott, L. Pfaff, U. T. Bornscheuer, A. Lendlein, R. Machatschek, *Chem. Catal.* **2022**, *2*, 3573–3589.
[38] T. Fecker, P. Galaz-Davison, F. Engelberger, Y. Narui, M. Sotomayor, L. P. Parra, C. A. Ramirez-Sarmiento, *Biophys. J.* **2018**, *114*, 1302.
[39] S. Kumar, C. J. Tsai, R. Nussinov, *Protein Eng.* **2000**, *13*, 179–191.
[40] E. Erickson, J. E. Gado, L. Avilán, F. Bratti, R. K. Brizendine, P. A. Cox, R. Gill, R. Graham, D.-J. Kim, G. König, W. E. Michener, S. Poudel, K. J. Ramirez, T. J. Shakespeare, M. Zahn, E. S. Boyd, C. M. Payne, J. L. DuBois,

A. R. Pickford, G. T. Beckham, J. E. McGeehan, *Nat. Commun.* **2022**, *13*, 7850.
[41] P. Puigbò, E. Guzmán, A. Romeu, S. Garcia-Vallvé, *Nucleic Acids Res.* **2007**, *35*, W126-W131.
[42] F. W. Studier, *Protein Expression Purif.* **2005**, *41*, 207–234.
[43] G. Winter, D. G. Waterman, J. M. Parkhurst, A. S. Brewster, R. J. Gildea, M. Gerstel, L. Fuentes-Montero, M. Vollmar, T. Michels-Clark, I. D. Young, N. K. Sauter, G. Evans, *Acta Crystallogr. D Struct. Biol.* **2018**, *74*, 85–97.
[44] J. M. Parkhurst, G. Winter, D. G. Waterman, L. Fuentes-Montero, R. J. Gildea, G. N. Murshudov, G. Evans, *J. Appl. Crystallogr.* **2016**, *49*, 1912–1921.
[45] A. Vagin, A. Teplyakov, *Acta Crystallogr. Sect. D* **2010**, *66*, 22–25.
[46] P. Emsley, B. Lohkamp, W. G. Scott, K. Cowtan, *Acta Crystallogr. Sect. D* **2010**, *66*, 486–501.
[47] G. N. Murshudov, P. Skubák, A. A. Lebedev, N. S. Pannu, R. A. Steiner, R. A. Nicholls, M. D. Winn, F. Long, A. A. Vagin, *Acta Crystallogr. Sect. D* **2011**, *67*, 355–367.
[48] C. J. Williams, J. J. Headd, N. W. Moriarty, M. G. Prisant, L. L. Videau, L. N. Deis, V. Verma, D. A. Keedy, B. J. Hintze, V. B. Chen, S. Jain, S. M. Lewis, W. B. Arendall, J. Snoeyink, P. D. Adams, S. C. Lovell, J. S. Richardson, D. C. Richardson, *Protein Sci.* **2018**, *27*, 293–315.
[49] D. A. Case, T. E. Cheatham, T. Darden, H. Gohlke, R. Luo, K. M. Merz, A. Onufriev, C. Simmerling, B. Wang, R. J. Woods, *J. Comput. Chem.* **2005**, *26*, 1668–1688.
[50] R. B. Best, X. Zhu, J. Shim, P. E. Lopes, J. Mittal, M. Feig, A. D. Mackerell, *J. Chem. Theory Comput.* **2012**, *8*, 3257–3273.
[51] S. Jo, T. Kim, V. G. Iyer, W. Im, *J. Comput. Chem.* **2008**, *29*, 1859–1865.
[52] W. F. van Gunsteren, H. J. C. Berendsen, *Mol. Phys.* **1977**, *34*, 1311–1327.
[53] P. J. Steinbach, B. R. Brooks, *J. Comput. Chem.* **1994**, *15*, 667–683.
[54] T. Darden, D. York, L. Pedersen, *J. Chem. Phys.* **1993**, *98*, 10089–10092.
[55] D. R. Roe, T. E. Cheatham, *J. Chem. Theory Comput.* **2013**, *9*, 3084–3095.
[56] B. R. Brooks, C. L. Brooks Iii, A. D. Mackerell Jr, L. Nilsson, R. J. Petrella, B. Roux, Y. Won, G. Archontis, C. Bartels, S. Boresch, A. Caflisch, L. Caves, Q. Cui, A. R. Dinner, M. Feig, S. Fischer, J. Gao, M. Hodoscek, W. Im, K. Kuczera, T. Lazaridis, J. Ma, V. Ovchinnikov, E. Paci, R. W. Pastor, C. B. Post, J. Z. Pu, M. Schaefer, B. Tidor, R. M. Venable, H. L. Woodcock, X. Wu, W. Yang, D. M. York, M. Karplus, *J. Comput. Chem.* **2009**, *30*, 1545–1614.

Manuscript received: December 7, 2022
Revised manuscript received: February 17, 2023
Accepted manuscript online: February 21, 2023
Version of record online: March 23, 2023